Arabian Journal of Chemistry 16 (2023) 105285

Contents lists available at ScienceDirect

Arabian Journal of Chemistry

journal homepage: www.sciencedirect.com

Original article

Heterogeneous activation of peroxymonosulfate by recyclable magnetic CuO/Fe_3O_4 nanosheets for efficient degradation of organic pollutants

Deyong Wu *, Xiangfei Li

School of Chemical and Environmental Engineering, Hubei Minzu University, Enshi, Hubei Province 445000, China

ARTICLE INFO

Article history:
Received 21 July 2023
Accepted 18 September 2023
Available online 22 September 2023

Keywords:
Magnetic
Peroxymonosulfate
Applicability
Mechanism

ABSTRACT

In this work, recyclable magnetic CuO/Fe_3O_4 nanosheetswere successfully synthesized via a simple continuous precipitation method, which can effectively activate peroxymonosulfate (PMS) to decompose organic pollutants. The properties of CuO/Fe_3O_4 nanosheets were measured by a series of characterization techniques. CuO/Fe_3O_4 composites showed highly effectiveness for PMS activation to degrade methyl blue (MB), and several influencing factors were investigated, such as initial pH, catalyst dosage, PMS concentration and reaction temperature. Although CuO/Fe_3O_4/PMS system exhibited effectiveness for MB degradation in a wide pH range, the natural pH value was the best. The increase in reaction temperature is favorable for MB degradation, and the activation energy was calculated as 40.34 kJ/mol. Quenching experiments and electron spin resonance (ESR) analysis proved that $^{\cdot}OH$, $SO_4^{\cdot-}$ and $^1O_2$ were generated in the CuO/Fe_3O_4/PMS system, and $SO_4^{\cdot-}$ and $^1O_2$ played the dominant role. Moreover, CuO/Fe_3O_4 remained good activity and stability after being recycled five times. In addition, the complete degradation of methylene orange (MO) and tetracycline hydrochloride (TC), and MB degradation in tap water and lake water further confirmed the wide applicability of the CuO/Fe_3O_4/PMS system. These results exhibited that CuO/Fe_3O_4/PMS system has great advantages of high removal efficiency, reusability and wide applicability, demonstrating its potential environmental application in the treatment of organic wastewater.

1. Introduction

Usually, biological processes may be the first choice in the wastewater treatment, because of the effectiveness and cost-effectiveness (Liu et al., 2022). However, conventional biological processes cannot effectively remove nonbiodegradable organic pollutants. So some new advanced oxidation processes (AOPs) have been developed to decompose the nonbiodegradable pollutants (Nguyen et al., 2020; Liu et al., 2023). Among them, sulfate radical ($SO_4^{\cdot-}$) based advanced oxidation processes (SR-AOPs) have received increased attention (Li et al., 2022; Zhu et al., 2023; Zhang et al., 2020). $SO_4^{\cdot-}$ has the higher oxidation potential and longer half-life than that of hydroxyl radical ($^{\cdot}OH$). Compared with H_2O_2, persulfate, including peroxymonosulfate (PMS) and peroxodisulfate (PDS), has lots of advantages, suach as lower cost, higher security, easier storage and transportation.

PMS is an asymmetric structure peroxide, which can be activated by carbon-based materials (Wang et al., 2023) transition metals (Wang et al., 2023), UV radiation (Guerra-Rodriguez et al., 2021); heat (Yin et al., 2022), ultrasound (Gujar et al., 2023); microwaves (Qi et al., 2017). Transition metal ions were used to activate PMS for the degradation of organic pollutants (Wang et al., 2023; Song et al., 2022; Mohammed Al-Balawi et al., 2023). But there are some insurmountable drawbacks for the homogeneous phase of transition metal ions; such as the high pH dependence, unrecyclable flaw. Metal oxides as heterogeneous catalysts can overcome the above drawbacks (Nguyen et al., 2023; Liu et al., 2023). Therefore, metal oxides have been intensively developed for PMS activation. For example, magnetic $CoFe_2O_4$ nanocrystals were prepared to activate PMS for the degradation of chloramphenicol (Yang et al., 2021) and for disinfection in different wastewater matrices (Rodriguez-Chueca et al., 2020). Nano-MoO_2 exhibited excellent performance in activating PMS and the MoO_2/PMS system can effectively remove naphthalene derivatives in aqueous systems (Chen et al., 2021). $CuMn_2O_4$ nanoparticles were utilized to activate PMS for the degradation of crystal violet (Farajollahi et al., 2023). Recently, CuO as PMS activator has

* Corresponding author.
E-mail address: wdy001815@126.com (D. Wu).
Peer review under responsibility of King Saud University.

Production and hosting by Elsevier

https://doi.org/10.1016/j.arabjc.2023.105285
1878-5352/

attracted much attention due to its abundant reserves, low price, simple preparation and high catalytic ability (Wei et al., 2022; Yan et al., 2021; Wang et al., 2021; Qin et al., 2020; Wang et al., 2019). Spongelike porous CuO exhibited good performance in activating PMS for the degradation of Acid Orange 7 (Qin et al., 2020). A series of metal oxides (ZnO, NiO, Al_2O_3, Fe_2O_3, MnO_2, CuO, CeO_2, La_2O_3) were synthesized by calcination method for PMS activation, and CuO showed a relatively higher performance in the degradation of 2, 6-dichlorophenol (Yan et al., 2021).

However, difficult recovery of CuO limited its application for PMS activation in aqueous systems. Therefore, the development of recyclable CuO-based heterogeneous catalysts is a meaningful thing. Due to the magnetic property, Fe_3O_4 was used as a support to obtain stable and magnetically recyclable heterogeneous catalysts (Li et al., 2023; Guo et al., 2023). Herein, CuO/Fe_3O_4 catalyst was prepared via a simple continuous precipitation method and used to activate PMS, which might simultaneously utilize the high catalytic property of CuO and the magnetic property of Fe_3O_4. The morphologies and properties of the CuO/Fe_3O_4 catalyst were systematically characterized by scanning electron microscopy (SEM), transmission electron microscopy (TEM), X-ray diffraction (XRD) and X-ray photoelectron spectroscopy (XPS). The catalytic performance of the CuO/Fe_3O_4 catalyst as PMS activator was evaluated through decomposing methyl blue (MB). Several influencing factors were investigated, such as initial pH, catalyst dosage, PMS concentration and reaction temperature. Furthermore, the applicability and stability of the CuO/Fe_3O_4 were also evaluated. In addition, the reactive oxygen species (ROS) generated in the CuO/Fe_3O_4/PMS were verified by the quenching experiment and EPR analysis.

2. Experimental section

2.1. Materials

Potassium peroxymonosulfate (PMS), Methylene blue (MB), Methyl Orange (MO), Tetracycline Hydrochloride (TC), isopropanol (IPA), *tert*-Butanol (TBA), L-Histidine (L-HIS), $FeSO_4{\cdot}7H_2O$, $CuSO_4{\cdot}5H_2O$, NaOH and HCl were obtained from Sinopharm Chemical Reagent Co., Ltd. All of the reagents and solvents used in the experiment were commercially obtained without any purification. Deionized water (DI water, 18.2 MΩcm) applied for preparing aqueous solutions.

2.2. Preparation of the catalysts

The Fe_3O_4 catalyst was fabricated using a simple method. Typically, 5.0 g $FeSO_4{\cdot}7H_2O$ was dissolved into 100 mL DI water under stirring. And pH value was adjusted to 12 using 1 mol/L NaOH solution. Then, the mixture was heated in a water bath at 70 ℃ for 2 h to obtain black precipitates of Fe_3O_4. The Fe_3O_4 precipitates were collected and cleaned with DI water and ethanol for four times each, followed by drying under vacuum at 70 ℃.

The CuO/Fe_3O_4 catalysts were prepared as follows: 200 mg as-prepared Fe_3O_4 was uniformly mixed with 100 mL DI water with the aid of ultrasound, a certain amount of $CuSO_4{\cdot}5H_2O$ was added into the solution under stirring. After 1 h, pH value of the mixture was adjusted to 12 using 1 mol/L NaOH solution. Then, the mixture was heated in a water bath at 70 ℃ for 2 h to obtain CuO/Fe_3O_4 catalysts. The CuO/Fe_3O_4 precipitates were collected and cleaned with DI water and ethanol for four times each, followed by drying under vacuum at 70 ℃. The molar ration of CuO to Fe_3O_4 were set to 2:1, 1:1, 1:2, respectively. And as-prepared catalyst were named as CuO/Fe_3O_4-2, CuO/Fe_3O_4-1, CuO/Fe_3O_4-0.5, respectively. If there is no special instruction, CuO/Fe_3O_4 appeared in the following section was CuO/Fe_3O_4-1.The CuO catalyst was prepared by the same process without adding Fe_3O_4.

2.3. Material characterization

X-ray powder diffraction (XRD) pattern of samples were recorded on a powder X-ray diffractometer (D/max-2200/PC, Rigaku Corporation, Japan) with Cu Ka radiation, operating at 40 kV and 30 mA, where λ = 0.15418 nm for the Cu Kα line. XPS experiments were carried out on a RBD upgraded PHI-5000C ESCA system (Perkin-Elmer, USA), the shift of the binding energy due to relative surface charging was corrected using the C 1s level at 284.6 eV as an internal standard. The structure and morphology of the coatings were investigated by the field emission scanning electron microscopy (FESEM, FEI SIRION 200, FEI, USA). The structure and the morphology of the catalyst powders were observed by Transmission Electron Microscope (TEM, JEM-100CX, JEOL, Japan).

2.4. Experimental procedure

The catalytic activity of CuO/Fe_3O_4 was evaluated by degrading MB in the presence of PMS. Typically, 0.01 g CuO/Fe_3O_4 was added into 100 mL MB solution (20 mg/L) under stirring. After adsorption equilibrium for 30 min, PMS solution was added to trigger the oxidation process. Under continuous stirring, samples were taken at interval time, and immediately filtrated by a 0.22 μm syringe. The filtered fluid was instantly analyzed by a UV–vis spectrometer at 664 nm to measure the MB concentration. Each experiment was replicated three times.

3. Results and discussion

3.1. Characterization of catalysts

The morphologies of CuO, Fe_3O_4 and CuO/Fe_3O_4 were characterized by SEM (Figs. S1-S3). CuO owned sheet shape with a smooth surface (Fig. S1), and most Fe_3O_4 particles were agglomerated together due to the magnetic force (Fig. S2). CuO/Fe_3O_4 also exhibited sheet shape, but the surface is obvious rough, and the shape is irregular compared to CuO (Fig. S3). In addition, CuO/Fe_3O_4 also showed the sheet shape observed from the TEM images of CuO/Fe_3O_4 (Fig. 1a), and the lattice lines of CuO and Fe_3O_4 can be observed clearly in HR-TEM image (Fig. 1b). The lattice lines of 0.235 nm and 0.292 nm should be attributed to the (111) crystal plane of CuO and the (220) crystal plane of Fe_3O_4, respectively. Furthermore, the elemental mapping test was carried out to further determine the composition of CuO/Fe_3O_4. According to the results (Fig. S4), Cu, Fe and O elements coexisted in the catalyst, and dispersed uniformly on the composite surface.

XRD patterns of CuO, Fe_3O_4 and CuO/Fe_3O_4 were shown in Fig. 2. For Fe_3O_4, a series of diffraction peaks at 30.1°, 35.4°, 43.1°, 53.6° and 57.1° are observed distinctly, corresponding to the (220), (311), (400), (422) and (511) planes of the Fe_3O_4 (JCPDS PDF No. 65–3107). (Cui et al., 2021; Chen et al., 2021; Yang et al., 2016) For CuO, the major diffraction peaks appeared at 32.4°, 35.5°, 38.7°, 48.7°, 53.5° and 58.2°, which should be attributed to the (110), (−111), (111), (−202), (020) and (202) planes of monoclinic structure of CuO (JCPDS 48–1548) (Li and Wu, 2022). For CuO/Fe_3O_4, the characteristic peaks of both CuO and Fe_3O_4 were presented clearly, indicating the successful preparation of CuO/Fe_3O_4 composites.

The chemical state of CuO/Fe_3O_4 surface was investigated by XPS, as shown in Fig. 3. In Cu 2p XPS spectra, two peaks at near 933.1 eV and 953.2 eV are belong to Cu $2p_{3/2}$ and Cu $2p_{1/2}$, respectively (Fig. 3a) And the other peaks at near can be assigned to the

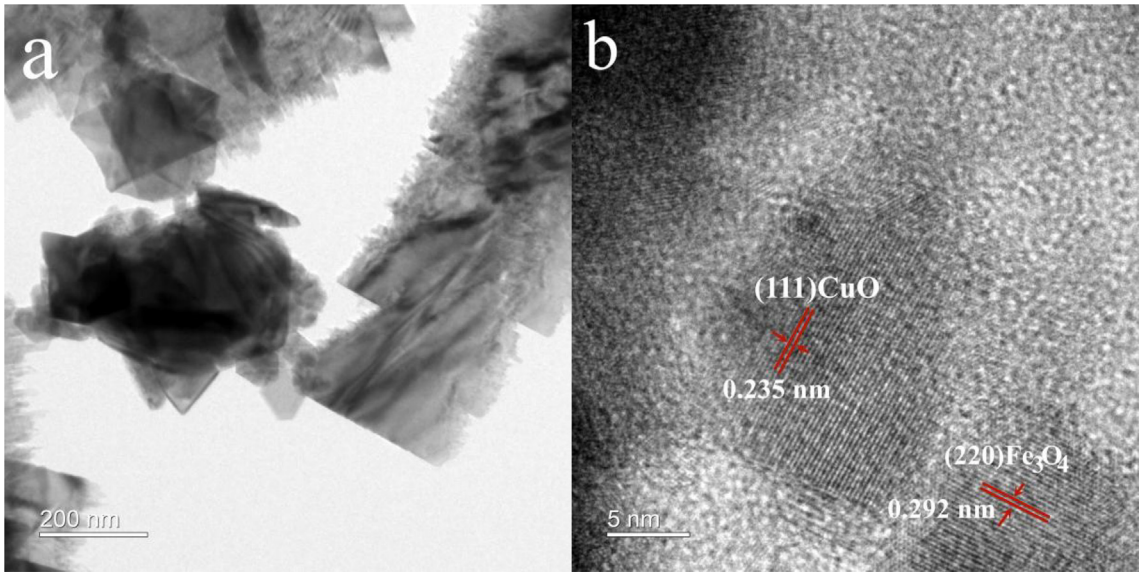

Fig. 1. TEM (a) and HR-TEM images (b) of CuO/Fe_3O_4 composites.

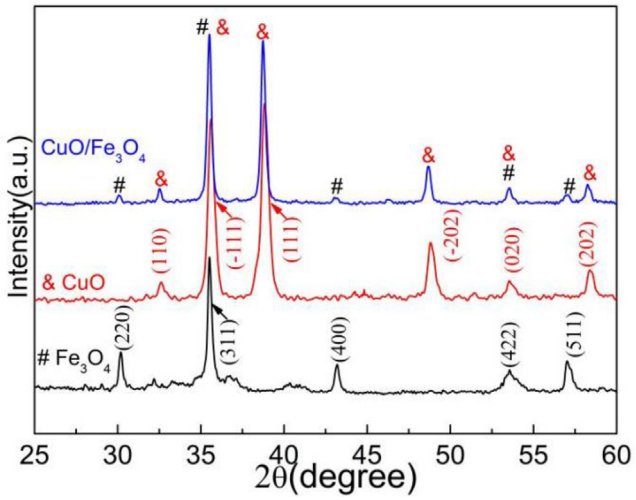

Fig. 2. XRD patterns of as-synthesized CuO, Fe_3O_4 and CuO/Fe_3O_4 composites.

satellite peaks of Cu 2p (Zuo et al., 2021; Xu et al., 2021). And the Auger peak at 568.73 eV further confirmed the presence of Cu^{2+} (Fig. 3b) (Zuo et al., 2021), indicating the existence of CuO rather than Cu_2O. The peaks of Fe $2p_{3/2}$ and Fe $2p_{1/2}$ of Fe_3O_4 at 711.7 eV and 723.8 eV with a satellite peak at 719.4 eV (Fig. 3c) (Cui et al., 2021; Singh et al., 2019). The peaks at near 529.8 eV and 531.4 eV in the O 1s spectra were attributed to the lattice oxygen and the adsorbed oxygen (Fig. 3d).

The catalytic performance of CuO/Fe_3O_4/PMS was explored by the degradation of MB. As shown in Fig. 4, the MB removal though the adsorption of CuO/Fe_3O_4 was negligible. The MB degradation by PMS without catalyst is no obvious. However, the CuO/Fe_3O_4/PMS system can realize the complete the MB degradation in 30 min. The results demonstrated that CuO/Fe_3O_4 can effectively activate PMS to decompose MB. Meanwhile, Fe_3O_4/PMS showed equally poor oxidation performance with a removal efficiency of only about 12% (Fig. S5). And the proportion of CuO in CuO/Fe_3O_4 composites is higher, the catalytic performance of CuO/Fe_3O_4/PMS is better for the degradation of MB. And all MB can be removed in 5 min by the CuO/PMS system (Fig. S5). Other studies also have verified that Fe_3O_4 has a weak catalytic activity to active PS or PMS, which often needs external energy, such as ultrasonic sound, ultraviolet light (Yang et al., 2021). These results certified that the outstanding performance of CuO/Fe_3O_4 for PMS activation should be attributed to CuO. And the main role of Fe_3O_4 is to provide the magnetic property for CuO/Fe_3O_4 composites in our work, which is very convenient to recover the catalyst.

The effects of CuO/Fe_3O_4 dosage and PMS concentration on the MB removal were studied, as shown in Fig. 5. MB degradation efficiency drastically enhanced with the increased CuO/Fe_3O_4 dosage (Fig. 5a). When 0.1 g/L of catalyst is added into the solution, it needs 30 min to completely remove MB. As the catalyst amount is increased to 0.20 g/L, MB can be completely removed in 10 min. Subsequently, the degradation rate can be continuously improved by adding more CuO/Fe_3O_4 dosage (0.30 g/L). The result is mainly because the increased catalyst may provide more reactive sites for PMS activation (Yang et al., 2021; Zhao et al., 2021). As a result, more reactive species can be produced for the rapid decomposition of MB. The effect of PMS concentration was showed in Fig. 5b. Firstly, the degradation rate of MB increased with the increase of PMS concentration form 1 mmol/L to 2 mmol/L. As a strong oxidant, PMS can be activated on the reactive sites of catalyst to generate ROS. The reactive sites on the surface of CuO/Fe_3O_4 will be more fully utilized with the increase of PMS dosage. Consequentially, more ROS can be produced to improve the removal efficiency of MB (Yang et al., 2021). However, the degradation rate of MB decreased later with the increase of PMS concentration form 2 mmol/L to 3 mmol/L. Excessive PMS can cause the self-quenching reactions of PMS (Liu et al., 2021; Ma et al., 2018). As described in Eqs. (1)–(3), excessive PMS will promote the conversion of ·OH and $SO_4^{\cdot-}$ to $SO_5^{\cdot-}$ and $\cdot HO_2$ with lower reactivity (Zhao et al., 2021; Liu et al., 2021).

$$\cdot OH + HSO_5^- \rightarrow SO_5^{\cdot-} + H_2O \quad (1)$$

$$SO_4^{\cdot-} + HSO_5^- \rightarrow SO_5^{\cdot-} + HSO_4^- \quad (2)$$

$$SO_4^{\cdot-} + HSO_5^- + H_2O \rightarrow HO_2\cdot + 2HSO_4^- \quad (3)$$

The pH value of the solution not only influences the existence form of PMS, but also the properties of the catalyst (Liu et al., 2023). So it is very important for the catalytic activity of the

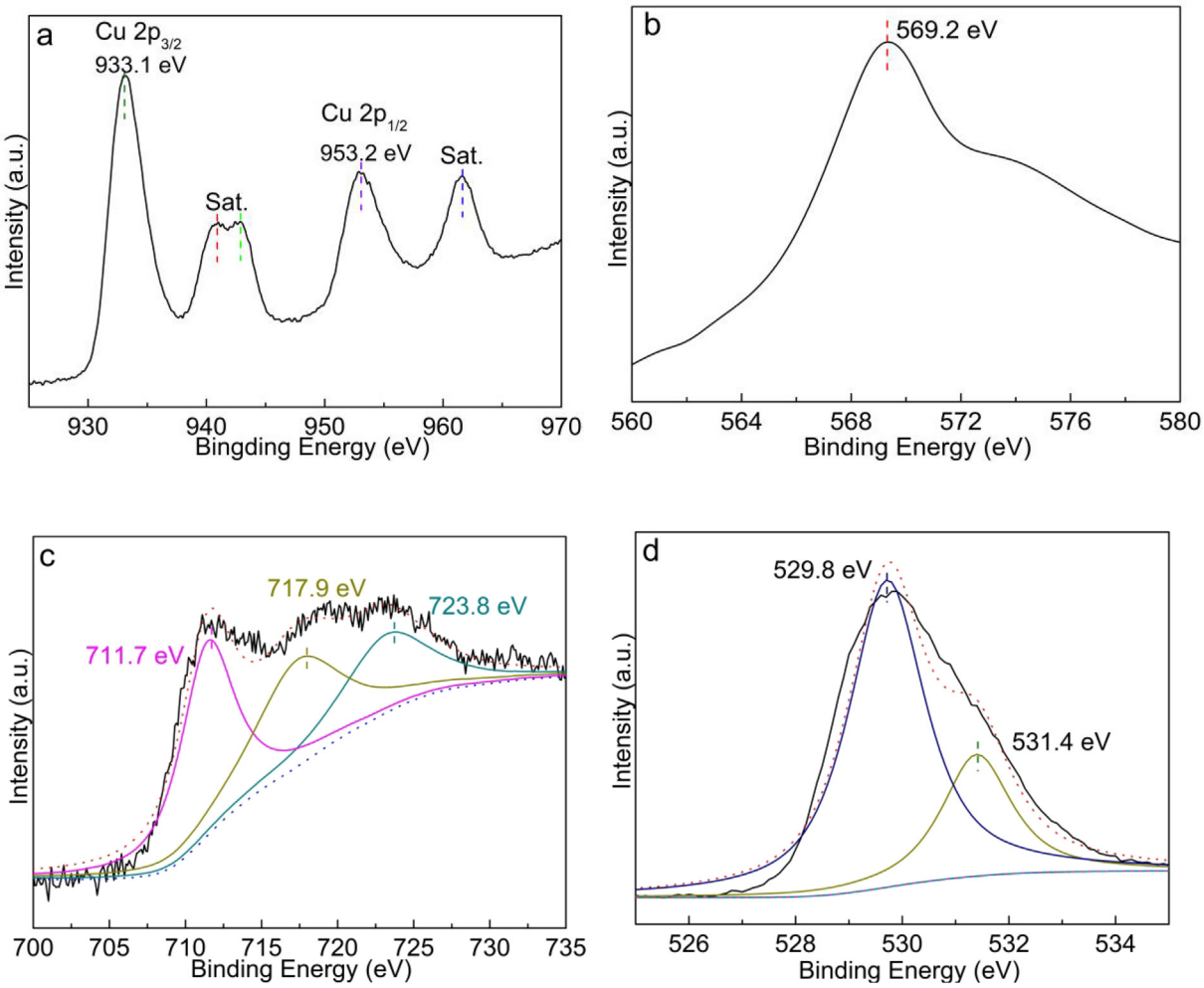

Fig. 3. XPS spectra of Cu 2p (a), Cu LMM (b), Fe 2p (c) and O 1s (d) of CuO/Fe_3O_4 composites.

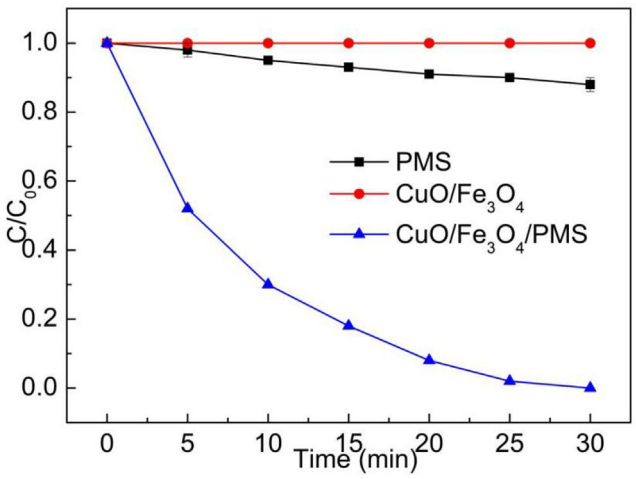

Fig. 4. Degradation of MB in various systems. Initial conditions: [MB] = 20 mg/L, [PMS] = 1 mmol/L, [CuO/Fe_3O_4] = 0.1 g/L, pH = 7.55.

CuO/Fe_3O_4/PMS system. To test the effect of initial pH on the MB degradation, different initial pH of solution was adjusted by adding 1 mol/L NaOH solution or 1 mol/L HCl solution. As presented in Fig. 6a, the removal efficiencies of MB were 14.1%, 63.3%, 100% and 85.2% in 30 min at pH 2.21, 4.40, 7.55 and 12.10, respectively. Meanwhile, as showed in Fig. S6, the MB removal basically followed the first order kinetic model (Eq. (4)), where C and C_0 represented the MB real-time and initial concentration, respectively, k_{obs} was the rate constant. Observed form Fig. 6b, the highest k_{obs} was acquired at a neutral pH (pH = 7.55).

$$\ln(C/C_0) = -k_{obs}t \quad (4)$$

In most cases, the highest degradation rate of pollutants via PMS/catalyst system is obtained under near-neutral conditions (Liu et al., 2023; Li and Wu, 2022; Zhen et al., 2021). Under acidic conditions, strong hydrogen bonds will be formed between excess H^+ with O-O in PMS, which inhibit the reaction between catalysts and PMS. Thus it depresses the formation of ROS, and further reduce the degradation of pollutant. Besides, metal ions from metal oxides are easy to dissolve into the reaction solution under acidic conditions. But the leaching ions always have a weaker ability for PMS activation. In our work, the extreme acidic condition (pH = 2.21) is bad for PMS activation by CuO/Fe_3O_4 composites. And the MB removal efficiency was very tiny (14.1%). Similar phenomenon was displayed in our previous work, the MB degradation in the CuO/PMS system was negligible under extreme acidic condition (pH ≈ 2) (Li and Wu, 2022). On the other hand, although the increasing of OH^-ions may accelerate PMS decomposition, the MB removal deceased from 100% at pH = 7.55 to 85.2% at pH = 12.10. The several reasons may lead to this result. Firstly, the pK_{a2} of PMS is 9.4, so PMS mainly exists in the form of SO_5^{2-}

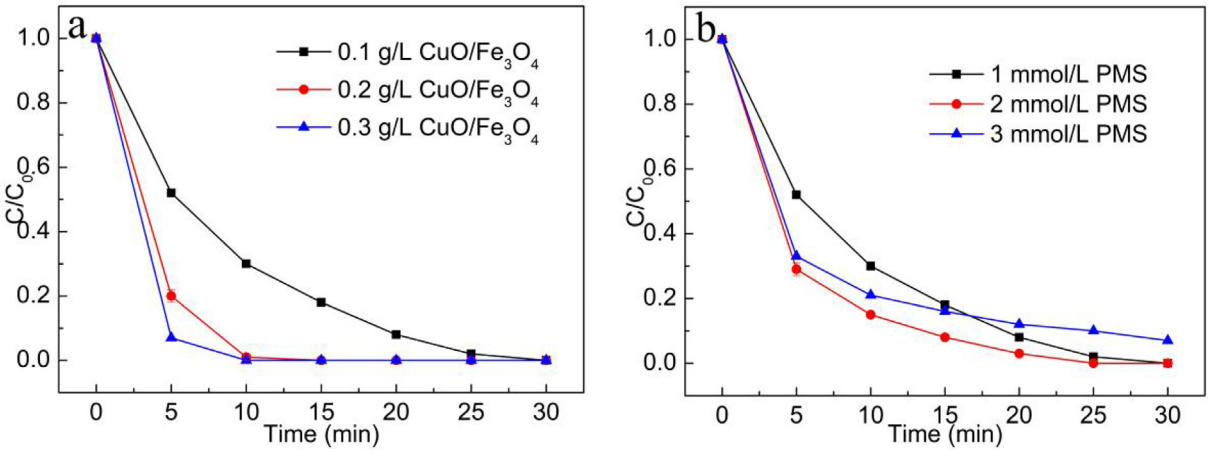

Fig. 5. The effect of CuO/Fe_3O_4 loading (a) and PMS concentration (b) on MB degradation. Initial conditions: [MB] = 20 mg/L, [PMS] = 1 mmol/L, [CuO/Fe_3O_4] = 0.1 g/L, pH = 7.55.

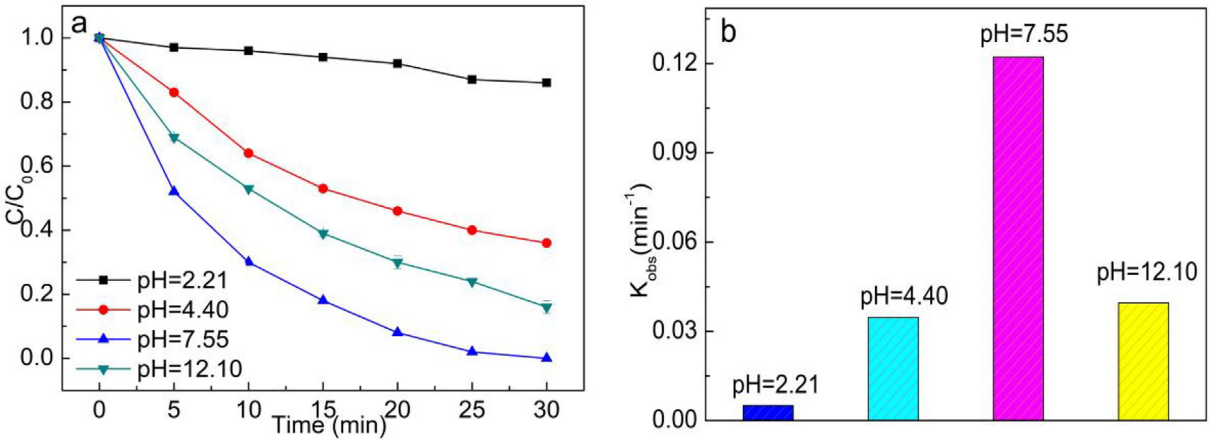

Fig. 6. The effect of initial pH value on MB removal (b) and degradation rates of MB in the CuO/Fe_3O_4/PMS system. Initial conditions: [MB] = 20 mg/L, [PMS] = 1 mmol/L, [CuO/Fe_3O_4] = 0.1 g/L.

under strongly alkaline conditions (pH = 12.10). The isoelectric point (pHpzc) of the CuO/Fe_3O_4 composite was about pH 8.8 (Zhen et al., 2021; Ding et al., 2020). Therefore, the surface of CuO/Fe_3O_4 catalyst was negative under strongly alkaline conditions (pH = 12.10). Consequentially, electrostatic repulsive forces are generated between PMS components and catalysts under strongly alkaline conditions (pH = 12.10), preventing the generation of ROS. Secondly, inactive materials such as SO_4^{2-} will be formed through the hydrolysis of PMS under basic conditions (Eq. (5)) (Rastogi et al., 2009). In addition,$SO_4^{\cdot-}$ was easily converted to ·OH under alkaline conditions (Eq. (6)), which had lower oxidation capacity and selectivity (Liu et al., 2023).

$$HSO_5^- + 2OH^- \rightarrow 2SO_4^{2-} + H_2O + O_2 \quad (5)$$

$$SO_4^{\cdot-} + OH^- \rightarrow SO_4^{2-} + \cdot OH \quad (6)$$

The operating temperature also affect the chemical reaction. Here the PMS activation at varying temperatures with/without CuO/Fe_3O_4 composites toward MB oxidation were comprehensively investigated. As presented in Fig. 7a, MB molecules can be degraded through thermally activated PMS without catalyst. The MB degradation rate was improved with the increase of reaction temperature. It was improved from 12.1% to 33.9% with increasing reaction temperature from 20 to 40 ℃. PMS can be activated by energy, and a higher reaction temperature can supply more energy to promote the decomposition of PMS into more ROS (Duan et al., 2018), resulting in the higher degradation of MB. Compared with the thermally activated PMS, the MB decomposition by PMS activation in the presence of CuO/Fe_3O_4 composites was greatly improved (Fig. 7a). Similarly, the catalytic activity was also enhanced with the increasing reaction temperature. It took 25 min to completely degrade MB at 20 ℃, while 10 min at 40 ℃. According to the first order kinetic model (Fig. S7), the rate constants were obtained. The rate constant is increased form 0.1223 min^{-1} at 20 °C to 0.3501 min^{-1} at 40 °C (Fig. S8). The molecular movement would be accelerated with the increase of temperature, the higher temperature may facilitate the mass transfer process of heterogeneous systems (Duan et al., 2018; Yu et al., 2022; Asif et al., 2021). In a word, the upper temperature is good for the MB degradation based on the above-mentioned reasons. In addition, the activation energy of this reaction measured by employing the Arrhenius equation (Eq. (7)) (Qin et al., 2020; Ma et al., 2018), where R is the molar gas constant (8.314472 J/(mol·K)), T is the temperature (K), k_{obs} was the rate constant. The curve between 1/T and ln k_{obs} was plotted (Fig. 7b), and calculated Ea value is about 40.34 kJ/mol. The Ea value is lower than those of reported PMS-based systems, such as Co_3O_4-Bi_2O_3/PMS (50.5 kJ/-

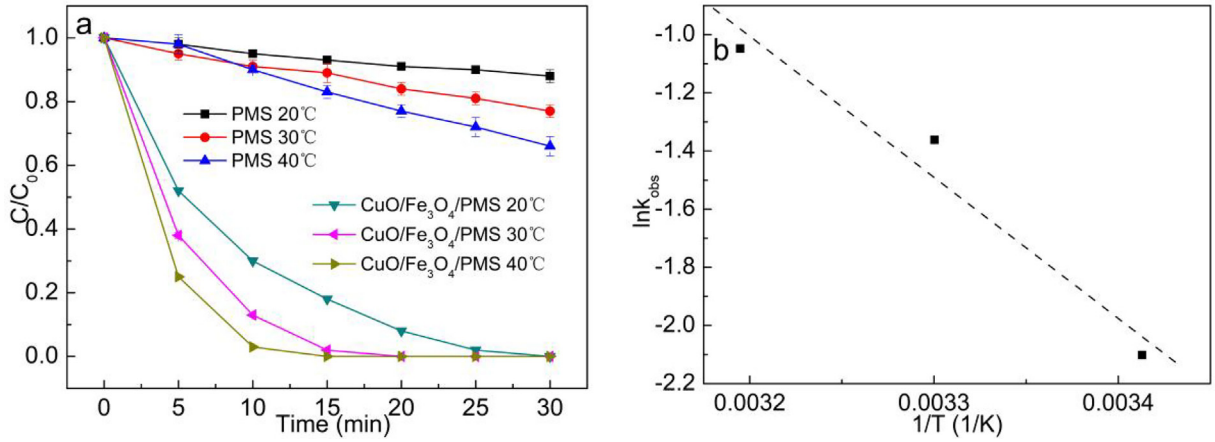

Fig. 7. The effect of reaction temperature on degradation rates of MB (a), and fitting of activation energy for CuO/Fe_3O_4/PMS system. Initial conditions: [MB] = 20 mg/L, [PMS] = 1 mmol/L, $[CuO/Fe_3O_4]$ = 0.1 g/L, pH = 7.55.

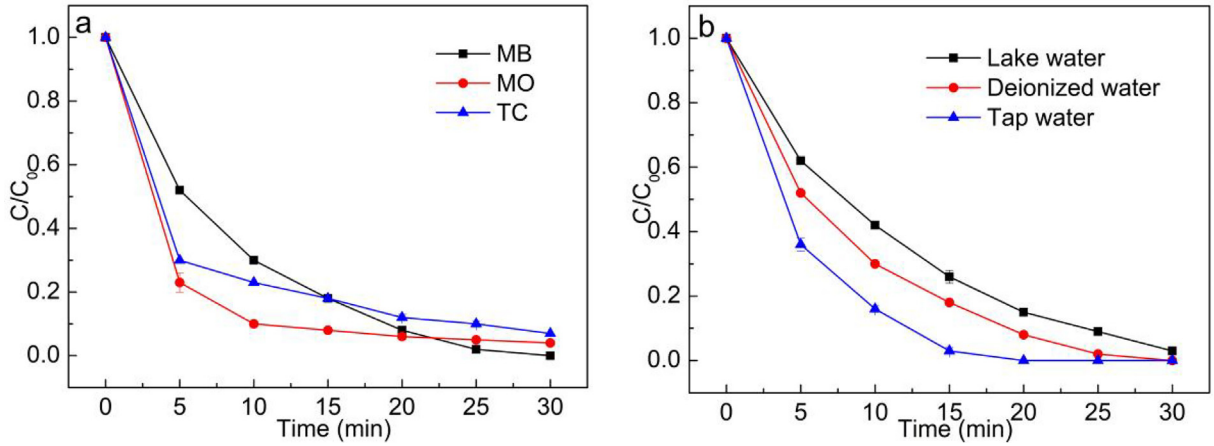

Fig. 8. Degradation of different pollutants in CuO/Fe_3O_4/PMS system (a), the effect of water bodies on MB degradation in CuO/Fe_3O_4/PMS system (b). Initial conditions: [MB/MO/TC] = 20 mg/L, [PMS] = 1 mmol/L, $[CuO/Fe_3O_4]$ = 0.1 g/L, pH = 7.55.

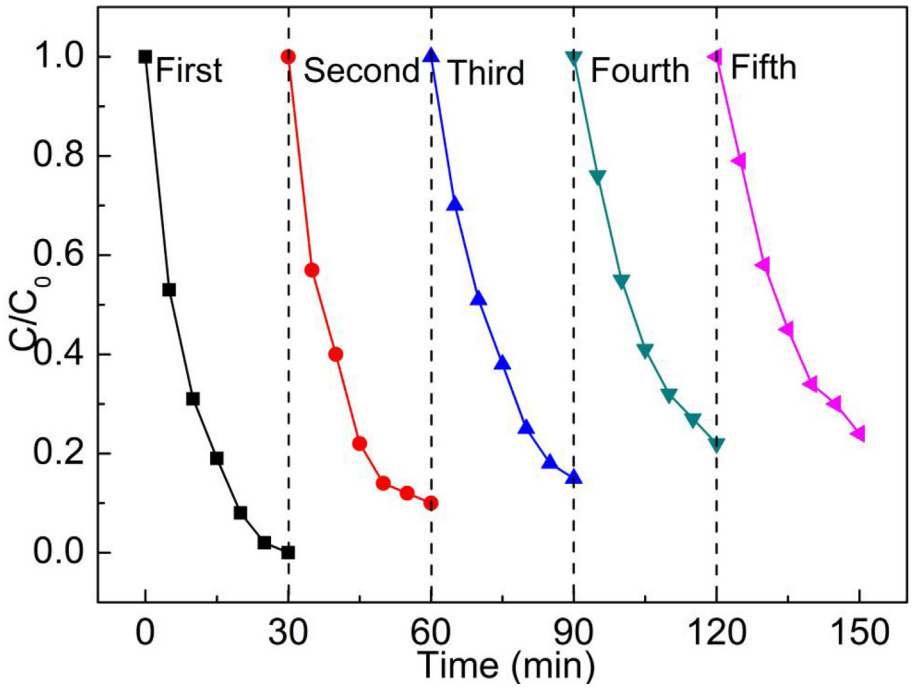

Fig. 9. Cycling tests of CuO/Fe_3O_4/PMS system toward MB degradation. Initial conditions: [MB] = 20 mg/L, [PMS] = 1 mmol/L, $[CuO/Fe_3O_4]$ = 0.1 g/L, pH = 7.55.

mol), CoMnAl-metal oxides/PMS (76.8 kJ/mol) and N-rGO/PMS (46.9 kJ/mol), indicating that the catalytic oxidation process in the CuO/Fe_3O_4/PMS system could be easily achieved (Qin et al., 2020).

$$\ln k_{obs} = \ln A - Ea/RT \quad (7)$$

To examine the wide applicability of this technology, the removal efficiencies of various organic pollutants and MB degradation efficiencies in different water bodies were explored respectively. Water bodies include tap water from our lab and lake water from the artificial lake on campus. MB, MO and TC were used as various organic pollutants. Details about the related process were described in the Supporting Information (Text S1 and Text S2). Fig. 8a presented the removal efficiencies of various organic pollutants in the CuO/Fe_3O_4/PMS system. Different pollutants have different molecular constructions and physicochemical characteristics, some differences in degradation efficiencies between pollutants are observed in the CuO/Fe_3O_4/PMS system. But all pollutants can be degraded effectively in CuO/Fe_3O_4/PMS system (Fig. S9). Surprisingly, it only took 10 min to degrade most of MO. Fig. 8b exhibited MB degradation efficiencies in different water matrices. Clearly, the removal efficiencies of MB in different water matrices all are nearly 100% (Fig. S10). The apparent rate constants for MB degradation were calculated by the pseudo first order kinetic model (Fig. S11). The k_{obs} values for MB degradation were 0.2266, 0.1468 and 0.1101 min^{-1} in TW, DW and LW, respectively (Fig. S12). What's more, the existence of positive ions in the MB solution, such as K^+, Ca^{2+}, Na^+, Mg^{2+}, had no inhibition for the removal of pollutants by the CuO/Fe_3O_4/PMS system (Fig. S13), other researches had got the similar phenomenons (Zhang et al., 2023; Zhong et al., 2022).

The stability and reusability of CuO/Fe_3O_4 composites were evaluated via cyclic experiment, which are very important for practical application. After each cycle, the used catalyst was collected by an external magnet (Fig. S14), and reused after drying. Details about the related process were described in the Supporting Information (Text S3). Observed from Fig. 9, the MB degradation efficiency was depressed along with the increase of number of cycle. The main reason should be that the pollutants adsorbed on the surface of CuO/Fe_3O_4 composites gradually accumulated each cycle, thereby hindering the interaction between CuO/Fe_3O_4 composites and PMS molecules to produce ROS (Yang et al., 2021). Satisfactorily, the MB degradation efficiency still remained 77.48% after five runs. Meanwhile, the XRD pattern of CuO/Fe_3O_4 composites has no remarkable change (Fig. S15). The results demonstrated that CuO/Fe_3O_4 composites have good stability and reusability, highlighting the practicability in water remediation.

To determine the species of generated ROS for the MB degradation, a quenching experiment was carried out in CuO/Fe_3O_4/PMS system. Isopropanol (IPA), *tert*-butyl alcohol (TBA) and L-histidine (L-HIS) were used as quenching reagents. TBA is a commonly used to quench ·OH, and IPA can synchronously quench ·OH and $SO_4^{\cdot-}$ (Wang et al., 2021). In addition, ·OH, $SO_4^{\cdot-}$ and $^1O_2$ all can be quenched by L-histidine, the k values are 5.0×10^9 $M^{-1}s^{-1}$, 2.5×10^9 $M^{-1}s^{-1}$ and 1.5×10^8 $M^{-1}s^{-1}$ for ·OH and $SO_4^{\cdot-}$ and $^1O_2$, respectively (Li et al., 2022). As depicted in Fig. 10a, the degradation efficiency of MB was slightly depressed in the CuO/Fe_3O_4/PMS system by adding TBA. When IPA and L-HIS were added into the system, the MB removal efficiency were reduced to 77.8% and 16.8%, respectively. According to the pseudo first order kinetic model (Fig. 10b), the calculated k_{obs} values were decreased form 0.1223 min^{-1} without quenching reagents to 0.1017, 0.0502, 0.0044 min^{-1} in the presence of TBA, IPA, L-HIS, respectively

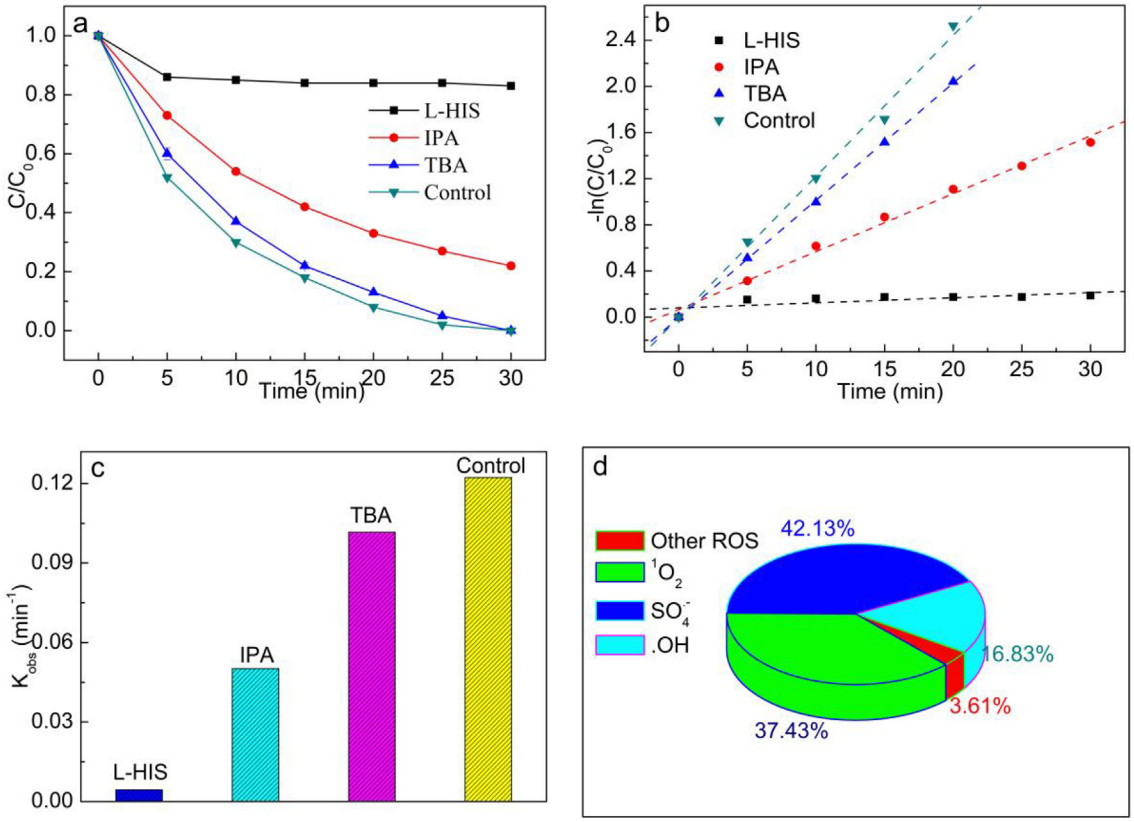

Fig. 10. MB degradation (a), pseudo-first-order kinetic curves for MB degradation (b) and MB degradation rate constants (c) in CuO/Fe_3O_4/PMS system in the presence of different scavengers. The contribution of ·OH, $SO_4^{\cdot-}$, $^1O_2$ and other ROS in CuO/Fe_3O_4/PMS system (d). Initial conditions: [MB] = 20 mg/L, [PMS] = 1 mmol/L, [CuO/Fe_3O_4] = 0.1 g/L, pH = 7.55, [IPA] = [TBA] = 50 mmol/L, [L-histidine] = 10 mmol/L.

(Fig. 10c). The k values of different quenching experiments were adopted for estimation of ROS contribution. The different ROS contributions were evaluated via Eqs. (8)–(11), where the k_0 represents the pristine rate constant in CuO/Fe_3O_4/PMS system, k_1, k_2, and k_3 were the kinetic constants of MB degradation with the addition of TBA, MeOH, and L-histidine, separately (Yu et al., 2022; Wang et al., 2020; Zhou et al., 2020). The results were presented in Fig. 10d. The results indicated that ·OH; $SO_4^{\cdot-}$ and $^1O_2$ all participated in the process, $SO_4^{\cdot-}$ and $^1O_2$ played the dominant role. And the ROS was further detected via EPR tests in CuO/Fe_3O_4/PMS system. As shown in Fig. 11, both signals of DMPO-·OH, DMPO-$SO_4^{\cdot-}$ and TEMP-$^1O_2$ were observed in CuO/Fe_3O_4/PMS system (Yu et al., 2022; Li et al., 2022; Ouyang et al., 2022).

$$\lambda(\cdot OH) = (k_0 - k_1)/k_0 \quad (8)$$

$$\lambda(SO_4^{\cdot-}) = (k_1 - k_2)/k \quad (9)$$

$$\lambda(^1O_2) = (k_2 - k_3)/k_0 \quad (10)$$

$$\lambda(\text{other ROS}) = k_3/k_0 \quad (11)$$

According to these results and some previously reported results (Yan et al., 2021; Zuo et al., 2021; Li et al., 2020; Li et al., 2019; Lei et al., 2015); the possible catalytic mechanism is illustrated in Fig. 12. Meanwhile, considering the dominant role of CuO in the CuO/Fe_3O_4 composites for PMS activation, the main reactions of producing ROS in the CuO/Fe_3O_4/PMS system were depicted as Eqs. (12)–(15). ≡Cu(Ⅱ) on the surface of CuO reacted with PMS to generate ≡Cu(Ⅲ) and $SO_4^{\cdot-}$ (Eq. (12)). The generated ≡Cu(Ⅲ) reacted with PMS to form $SO_5^{\cdot-}$ (Eq. (13)). In addition, the generated $SO_4^{\cdot-}$ can interact with H_2O to produce ·OH (Eq. (15)), the self-reaction of $SO_5^{\cdot-}$ will form $^1O_2$ (Eq. (16)). Subsequently, these ROS decomposed MB molecules inoto intermediates and mineralization products (CO_2 and H_2O) (Eq. (16)).

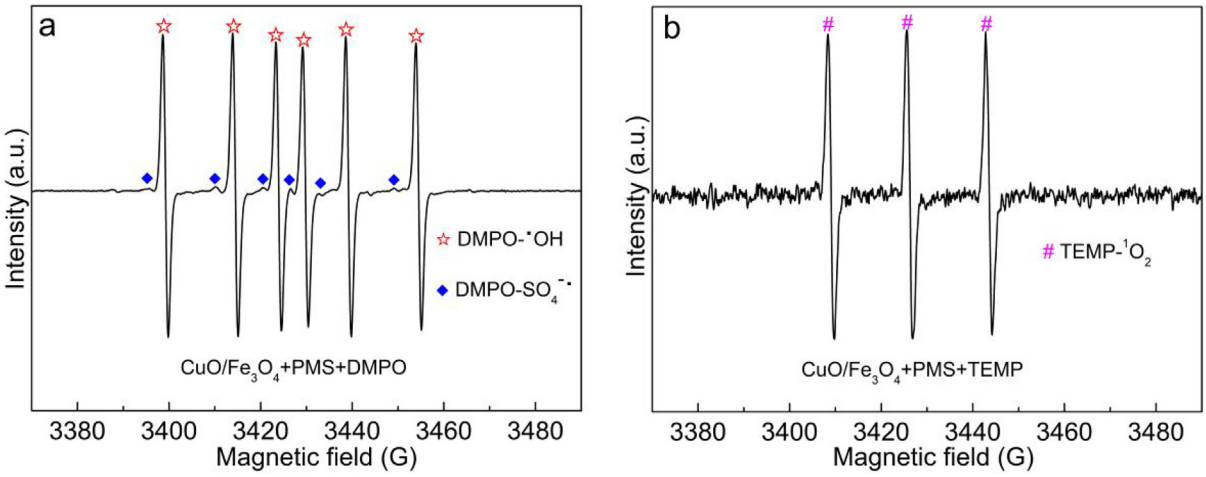

Fig. 11. EPR spectra of ·OH and $SO_4^{\cdot-}$ (a) and $^1O_2$ (b) in CuO/Fe_3O_4/PMS system.

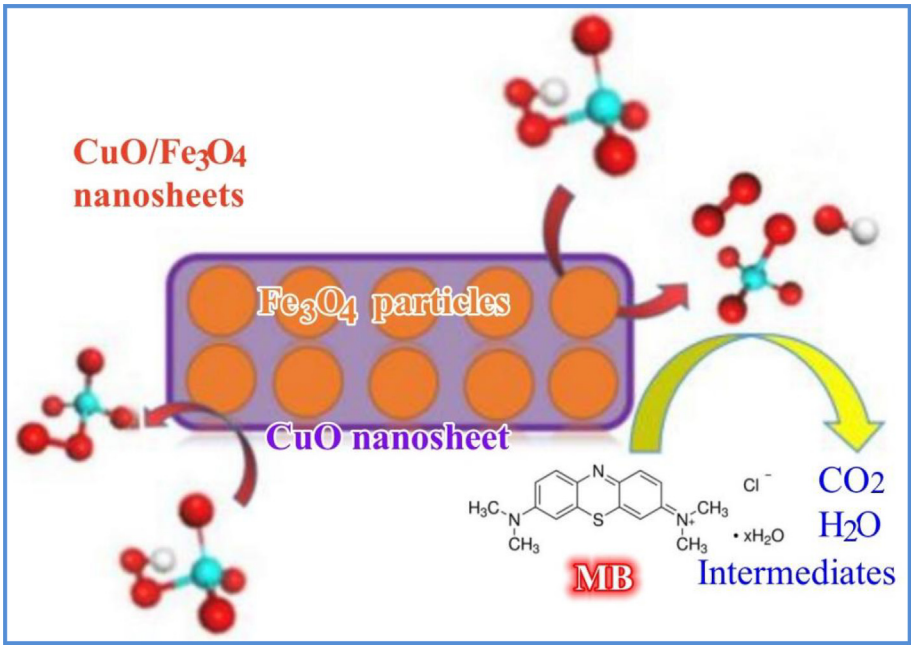

Fig. 12. Possible mechanism of MB degradation in the CuO/Fe_3O_4/PMS system.

$$\equiv Cu() + HSO_5^- \rightarrow \equiv Cu() + SO_4^{\cdot -} + OH^- \quad (12)$$

$$\equiv Cu() + HSO_5^- \rightarrow \equiv Cu() + SO_5^{\cdot -} + H^+ \quad (13)$$

$$SO_4^{\cdot -} + H_2O \rightarrow SO_4^{2-} + \cdot OH + H^+ \quad (14)$$

$$SO_5^{\cdot -} + SO_5^{\cdot -} \rightarrow SO_4^{2-} + {}^1O_2 \quad (15)$$

$$MB + SO_4^{\cdot -}/\cdot OH/{}^1O_2 \rightarrow CO_2 + H_2O + \text{intermediates} \quad (16)$$

4. Conclusion

In summary, magnetic CuO/Fe_3O_4 nanosheets were facilely synthesized for PMS activation to achieve high-efficient degradation of organic pollutants. CuO/Fe_3O_4 showed the good catalytic performance in a wide pH range (4–12). Higher dosages of CuO/Fe_3O_4, appropriate PMS concentration, higher reaction temperature and the neutral solution pH value were beneficial for MB removal. The radical quenching test and ESR showed that ·OH, $SO_4^{\cdot -}$ and $^1O_2$ were generated in the CuO/Fe_3O_4/PMS system, and $SO_4^{\cdot -}$ and $^1O_2$ played the main role. In addition, CuO/Fe_3O_4 could be collected by magnetic separation and reused with good performance. Moreover, other organic pollutants can be degraded completely in CuO/Fe_3O_4/PMS system, and CuO/Fe_3O_4/PMS system exhibited satisfactory removal of MB in real water matrix. In a word, high removal efficiency, the stability, reusability and wide applicability of CuO/Fe_3O_4/PMS were good for its utilization in the environmental remediation.

CRediT authorship contribution statement

Deyong Wu: Conceptualization, Methodology, Writing – original draft, Writing – review & editing. **Xiangfei Li:** Methodology, Investigation.

Declaration of Competing Interest

The authors declare that they have no known competing financial interests or personal relationships that could have appeared to influence the work reported in this paper.

Acknowledgment

This work was supported by the National Natural Science Foundation of China (Grant No. 21767009) and Hubei Minzu University (Grant No. PY21014).

Appendix A. Supplementary material

Supplementary data to this article can be found online at https://doi.org/10.1016/j.arabjc.2023.105285.

References

Asif, M.B., Ji, B., Maqbool, T., Zhang, Z., 2021. Algogenic organic matter fouling alleviation in membrane distillation by peroxymonosulfate (PMS): role of PMS concentration and activation temperature. Desalination 516, 115225.
Chen, X.W., Vione, D., Borch, T., Wang, J., Gao, Y.Z., 2021. Nano-MoO_2 activates peroxymonosulfate for the degradation of PAH derivatives. Water Res. 192, 116834.
Chen, M., Wang, N., Wang, X., Zhou, Y., Zhu, L., 2021. Enhanced degradation of tetrabromobisphenol A by magnetic Fe_3O_4@ZIF-67 composites as a heterogeneous Fenton-like catalyst. Chem. Eng. J. 413, 127539.
Cui, X.W., Zhang, S.S., Geng, Y., Zhen, J.Y., Zhan, J.H., Cao, C.B., Ni, S.Q., 2021. Synergistic catalysis by Fe_3O_4-biochar/peroxymonosulfate system for the removal of bisphenol a. Sep. Purif. Technol. 276, 119351.
Ding, Y., Pan, C., Peng, X., Mao, Q., Xiao, Y., Fu, L., Huang, J., 2020. Deep mineralization of bisphenol A by catalytic peroxymonosulfate activation with nano CuO/Fe_3O_4 with strong Cu-Fe interaction. Chem. Eng. J. 384, 123378.
Duan, X., Indrawirawan, S., Kang, J., Tian, W., Zhang, H., Sun, H., Wang, S., 2018. Temperature-dependent evolution of hydroxyl radicals from peroxymonosulfate activation over nitrogen-modified carbon nanotubes. Sustain. Mater. Techno. 18, e00082.
Farajollahi, A., Marjani, A.P., Pesyan, N.N., Alamgholiloo, H., 2023. Efficient degradation of crystal violet by $GO/CuMn_2O_4$ nanocomposite via peroxymonosulfate activation. Appl. Surf. Sci. 622, 156903.
Guerra-Rodriguez, S., Lado Ribeiro, A.R., Ribeiro, R.S., Rodriguez, E., Silva, A.M.T., Rodriguez-Chueca, J., 2021. UV-A activation of peroxymonosulfate for the removal of micropollutants from secondary treated wastewater. Sci. Total Environ. 770, 145299.
Gujar, S.K., Divyapriya, G., Gogate, P.R., Nidheesh, P.V., 2023. Environmental applications of ultrasound activated persulfate/peroxymonosulfate oxidation process in combination with other activating agents. Crit. Rev. Env. Sci. Tec. 53, 780–802.
Guo, Z., Lv, Y., Wei, J., Zhang, J., Song, Y., 2023. Efficient removal of sulfamethazine by a magnetic recoverable CeO_2/Fe_3O_4/natural zeolite catalyst in catalytic ozonation process. Front. Env. Sci. 11, 1137137.
Lei, Y., Chen, C.-S., Tu, Y.-J., Huang, Y.-H., Zhang, H., 2015. Heterogeneous degradation of organic pollutants by persulfate activated by $CuO-Fe_3O_4$: mechanism, stability, and effects of pH and bicarbonate ions. Environ. Sci. Tech. 49, 6838–6845.
Li, W.W., Cheng, L., Liu, J., Yang, S.Y., Zan, S.T., Zhao, G.C., 2023. Recyclable magnetic Fe_3O_4@C for methylene blue removal under microwave-induced reaction system. Chemosphere 310, 136821.
Li, X., Wu, D., 2022. Facile fabrication of CuO for removal of organic pollutants through peroxymonosulfate activation. Mater. Lett. 328, 133168.
Li, X., Jie, B., Lin, H., Deng, Z., Qian, J., Yang, Y., Zhang, X., 2022. Application of sulfate radicals-based advanced oxidation technology in degradation of trace organic contaminants (TrOCs): recent advances and prospects. J. Environ. Manage. 308, 114664.
Li, Z.D., Liu, D.F., Zhao, Y.X., Li, S.R., Wei, X.C., Meng, F.S., Huang, W.L., Lei, Z.F., 2019. Singlet oxygen dominated peroxymonosulfate activation by $CuO-CeO_2$ for organic pollutants degradation: Performance and mechanism. Chemosphere 233, 549–558.
Li, R., Lu, X., Yan, B., Li, N., Chen, G., Cheng, Z., Hou, L.A., Wang, S., Duan, X., 2022. Sludge-derived biochar toward sustainable Peroxymonosulfate activation: regulation of active sites and synergistic production of reaction oxygen species. Chem. Eng. J. 440, 135897.
Li, Z.D., Sun, Y.M., Huang, W.L., Xue, C., Zhu, Y., Wang, Q.W., Liu, D.F., 2020. Innovatively employing magnetic CuO nanosheet to activate peroxymonosulfate for the treatment of high-salinity organic wastewater. J. Environ. Sci. 88, 46–58.
Liu, T., Cui, K., Chen, Y., Li, C., Cui, M., Yao, H., Chen, Y., Wang, S., 2021. Removal of chlorophenols in the aquatic environment by activation of peroxymonosulfate with nMnOx@Biochar hybrid composites: Performance and mechanism. Chemosphere 283, 131188.
Liu, T., Cui, K., Li, C.-X., Chen, Y., Wang, Q., Yuan, X., Chen, Y., Liu, J., Zhang, Q., 2023. Efficient peroxymonosulfate activation by biochar-based nanohybrids for the degradation of pharmaceutical and personal care products in aquatic environments. Chemosphere 311, 137084.
Liu, H., Dai, X., Kong, L., Sui, C., Nie, Z., Liu, Y., Cai, B., Ni, S.Q., Boczkaj, G., Zhan, J., 2023. Ball milling treatment of Mn_3O_4 regulates electron transfer pathway for peroxymonosulfate activation. Chem. Eng. J. 467, 143339.
Liu, J., Wu, J., Wang, N., Tian, F., Li, J., 2022. Surface reconstruction of BiSI nanorods for superb photocatalytic Cr(VI) reduction under near-infrared light irradiation. Chem. Eng. J. 435, 135152.
Ma, W., Wang, N., Fan, Y., Tong, T., Han, X., Du, Y., 2018. Non-radical-dominated catalytic degradation of bisphenol A by ZIF-67 derived nitrogen-doped carbon nanotubes frameworks in the presence of peroxymonosulfate. Chem. Eng. J. 336, 721–731.
Mohammed Al-Balawi, A., Zaheer, Z., Kosa, S.A., 2023. Silver-platinum bimetallic nanoparticles as heterogeneous persulfate activator for the oxidation of malachite green. Arab. J. Chem. 16, 104863.
Nguyen, A.Q.K., Ahn, Y.Y., Shin, G., Cho, Y., Lim, J., Kim, K., Kim, J., 2023. Degradation of organic compounds through both radical and nonradical activation of peroxymonosulfate using $CoWO_4$ catalysts. Appl Catal B 324, 122266.
Nguyen, V.H., Smith, S.M., Wantala, K., Kajitvichyanukul, P., 2020. Photocatalytic remediation of persistent organic pollutants (POPs): a review. Arab. J. Chem. 13, 8309–8337.
Ouyang, D., Chen, Y., Chen, R., Zhang, W., Yan, J., Gu, M., Li, J., Zhang, H., Chen, M., 2022. Degradation of 1,4-dioxane by biochar activating peroxymonosulfate under continuous flow conditions. Sci. Total Environ. 809, 151929.
Qi, C., Liu, X., Lin, C., Zhang, H., Li, X., Ma, J., 2017. Activation of peroxymonosulfate by microwave irradiation for degradation of organic contaminants. Chem. Eng. J. 315, 201–209.
Qin, Q.D., Qiao, N., Liu, Y.H., Wu, X., 2020. Spongelike porous CuO as an efficient peroxymonosulfate activator for degradation of Acid Orange 7. Appl. Surf. Sci. 521, 117783.
Rastogi, A., Al-Abed, S.R., Dionysiou, D.D., 2009. Sulfate radical-based ferrous–peroxymonosulfate oxidative system for PCBs degradation in aqueous and sediment systems. Appl. Catal. B 85, 171–179.

Rodriguez-Chueca, J., Barahona-Garcia, E., Blanco-Gutierrez, V., Isidoro-Garcia, L., Dos Santos-Garcia, A.J., 2020. Magnetic $CoFe_2O_4$ ferrite for peroxymonosulfate activation for disinfection of wastewater. Chem. Eng. J. 398, 125606.

Singh, P., Sudhaik, A., Raizada, P., Shandilya, P., Sharma, R., Hosseini-Bandegharaei, A., 2019. Photocatalytic performance and quick recovery of BiOI/Fe_3O_4@graphene oxide ternary photocatalyst for photodegradation of 2,4-dintirophenol under visible light. Mater. Today Chem. 12, 85–95.

Song, H., Pan, S., Wang, Y., Cai, Y., Zhang, W., Shen, Y., Li, C., 2022. MXene-mediated electron transfer in Cu(II)/PMS process: from Cu(III) to Cu(I). Sep. Purif. Technol. 297, 121428.

Wang, M., Jin, C.Y., Kang, J., Liu, J.Y., Tang, Y.W., Li, Z.L., Li, S.Y., 2021. CuO/g-C_3N_4 2D/2D heterojunction photocatalysts as efficient peroxymonosulfate activators under visible light for oxytetracycline degradation: characterization, efficiency and mechanism. Chem. Eng. J. 416, 128118.

Wang, J., Shen, M., Wang, H.L., Du, Y.S., Zhou, X.Q., Liao, Z.W., Wang, H.B., Chen, Z.Q., 2020. Red mud modified sludge biochar for the activation of peroxymonosulfate: singlet oxygen dominated mechanism and toxicity prediction. Sci. Total Environ. 740, 140388.

Wang, S.X., Tian, J.Y., Wang, Q., Xia, F., Gao, S.S., Shi, W.X., Cui, F.Y., 2019. Development of CuO coated ceramic hollow fiber membrane for peroxymonosulfate activation: a highly efficient singlet oxygen-dominated oxidation process for bisphenol a degradation. Appl Catal B 256, 117783.

Wang, S.X., Tian, J.Y., Jia, L.R., Jia, J.L., Shan, S.J., Wang, Q., Cui, F.Y., 2021. Removal of aqueous organic contaminants using submerged ceramic hollow fiber membrane coupled with peroxymonosulfate oxidation: comparison of CuO catalyst dispersed in the feed water and immobilized on the membrane. J. Membr. Sci. 618, 118707.

Wang, S., Wang, K., Cao, W., Qiao, L., Peng, X., Yu, D., Wang, S., Li, C., Wang, C., 2023. Degradation of methylene blue by ellipsoidal B-FeOOH@MnO_2 core-shell catalyst: performance and mechanism. Appl. Surf. Sci. 619, 156667.

Wang, S.Y., Xia, Y., Tan, L., Wu, S.D., Yu, Y.L., Yu, X.P., Guan, Z., Chen, H., Jiang, F., 2023. Unraveling the instability of Nitrogen-Doped carbon during BPA treatment by peroxymonosulfate activation: effect of free radical grafting. Sep. Purif. Technol. 317, 123973.

Wei, Y., Miao, J., Ge, J., Lang, J., Yu, C., Zhang, L., Alvarez, P.J.J., Long, M., 2022. Ultrahigh peroxymonosulfate utilization efficiency over CuO Nanosheets via heterogeneous Cu(III) formation and preferential electron transfer during degradation of phenols. Environ. Sci. Tech. 56, 8984–8992.

Xu, W.J., Chen, X., Chen, J., Jia, H.P., 2021. Bimetal oxide CuO/Co_3O_4 derived from Cu ions partly-substituted framework of ZIF-67 for toluene catalytic oxidation. J. Hazard. Mater. 403, 123869.

Yan, P.W., Shen, J.M., Wang, S.Y., Zhou, Y.C., Kang, J., Yuan, L., Bi, L.B., Li, Y.B., Chen, Z. L., 2021. Removal of 2,6-dichlorophenol in water by CuO activated peroxymonosulfate: efficiency, mechanism and degradation pathway. Sep. Purif. Technol. 254, 117630.

Yang, H., Luo, B.H., Lei, S.H., Wang, Y.Y., Sun, J.F., Zhou, Z.J., Zhang, Y., Xia, S.B., 2021. Enhanced humic acid degradation by Fe_3O_4/ultrasound-activated peroxymonosulfate: synergy index, non-radical effect and mechanism. Sep. Purif. Technol. 264, 118466.

Yang, L.X., Yang, J.C.E., Fu, M.L., 2021. Magnetic CoFe2O4 nanocrystals derived from MIL-101 (Fe/Co) for peroxymonosulfate activation toward degradation of chloramphenicol. Chemosphere 272, 129567.

Yang, Q., Zhao, Q., Ren, S., Lu, Q., Guo, X., Chen, Z., 2016. Fabrication of core-shell Fe_3O_4@MIL-100(Fe) magnetic microspheres for the removal of Cr(VI) in aqueous solution. J. Solid State Chem. 244, 25–30.

Yin, L., Wei, J., Qi, Y., Tu, Z., Qu, R., Yan, C., Wang, Z., Zhu, F., 2022. Degradation of pentachlorophenol in peroxymonosulfate/heat system: kinetics, mechanism, and theoretical calculations. Chem. Eng. J. 434, 145299.

Yu, Y., Li, N., Wang, C., Cheng, Z., Yan, B., Chen, G., Hou, L.A., Wang, S., 2022. Iron cobalt and nitrogen co-doped carbonized wood sponge for peroxymonosulfate activation: performance and internal temperature-dependent mechanism. J. Colloid Interface Sci. 619, 267–279.

Zhang, X., Liu, J., Zhang, H., Wan, Z., Li, J., 2023. Uncovering the pathway of peroxymonosulfate activation over $Co_{0.5}Zn_{0.5}O$ nanosheets for singlet oxygen generation: performance and membrane application. Appl. Catal., B 327, 122429.

Zhang, H., Nengzi, L.C., Liu, Y., Gao, Y., Cheng, X., 2020. Efficient removal of organic pollutant by activation of persulfate with magnetic Co_3O_4/$CoFe_2O_4$ composite. Arab. J. Chem. 13, 5332–5344.

Zhao, C.H., Shao, B.B., Yan, M., Liu, Z.F., Liang, Q.H., He, Q.Y., Wu, T., Liu, Y., Pan, Y., Huang, J., Wang, J.J., Liang, J., Tang, L., 2021. Activation of peroxymonosulfate by biochar-based catalysts and applications in the degradation of organic contaminants: a review. Chem. Eng. J. 416, 128829.

Zhen, J., Zhang, S., Zhuang, X., Ahmad, S., Lee, T., Si, H., Cao, C., Ni, S.Q., 2021. Sulfate radicals based heterogeneous peroxymonosulfate system catalyzed by CuO-Fe_3O_4-Biochar nanocomposite for bisphenol A degradation. J. Water Process Eng. 41, 102078.

Zhong, Q., Liu, J., Wang, J., Li, Y., Li, J., Zhang, G., 2022. Efficient degradation of organic pollutants by activated peroxymonosulfate over TiO_2@C decorated Mg–Fe layered double oxides: Degradation pathways and mechanism. Chemosphere 2022, (300) 134564.

Zhou, X., Luo, C., Luo, M., Wang, Q., Wang, J., Liao, Z., Chen, Z., Chen, Z., 2020. Understanding the synergetic effect from foreign metals in bimetallic oxides for PMS activation: a common strategy to increase the stoichiometric efficiency of oxidants. Chem. Eng. J. 381, 122587.

Zhu, C., Cun, F., Fan, Z., Nie, Y., Du, Q., Liu, F., Yang, W., Li, A., 2023. Heterogeneous Fe-Co dual-atom catalyst outdistances the homogeneous counterpart for peroxymonosulfate-assisted water decontamination: new surface collision oxidation path and diatomic synergy. Water Res. 241, 120164.

Zuo, S.Y., Guan, Z.Y., Xia, D.S., Yang, F., Xu, H.M., Huang, M.Z., Li, D.Y., 2021. Polarized heterogeneous CuO-CN for peroxymonosulfate nonradical activation: an enhancement mechanism of mediated electron transfer. Chem. Eng. J. 420, 127619.